

# Flower-like ZnO grown on urchin-like CuO microspheres for catalytic synthesis of dimethyldichlorosilane†

Cite this: DOI: 10.1039/c3ra00171g

Yongxia Zhu,<sup>ab</sup> Yingli Wang,<sup>\*b</sup> Lianying Song,<sup>b</sup> Xin Chen,<sup>b</sup> Wuyuan Liu,<sup>b</sup> Jin Sun,<sup>a</sup> Xilin She,<sup>\*a</sup> Ziyi Zhong<sup>c</sup> and Fabing Su<sup>\*b</sup>

We report the rational growth of flower-like ZnO on urchin-like CuO (f-ZnO@u-CuO) microspheres *via* a facile solvothermal method using copper nitrate and zinc nitrate as precursors in the presence of sodium nitrate and ethanol. A formation mechanism was proposed based on the observation of a series of reaction intermediates. The samples were characterized by X-ray diffraction, transmission electron microscopy, scanning electron microscopy with energy-dispersive X-ray spectroscopy, X-ray photoelectron spectroscopy, inductively coupled plasma optical emission spectrometer, and temperature-programmed reduction. It was found that the morphology of the samples was highly dependent on the synthesis conditions, particularly the reaction time and the ammonia amount added. As a copper-based catalyst for dimethyldichlorosilane synthesis *via* the Rochow reaction, f-ZnO@u-CuO microspheres show better catalytic performance than the Cu-based catalysts physically mixed with ZnO promoter, probably because of the well-developed p-n heterojunction structures at the CuO and ZnO interfaces that generate a much strong synergistic effect. The work provides a simple method to synthesize hierarchical CuO/ZnO composites and would be helpful for understanding the catalytic mechanism of the Rochow reaction.

Received 13th January 2013,

Accepted 3rd April 2013

DOI: 10.1039/c3ra00171g

[www.rsc.org/advances](http://www.rsc.org/advances)

## 1. Introduction

As a p-type semiconductor, CuO has a narrow band gap ( $E_g = 1.2 \text{ eV}^{1-3}$ ) and is widely used as catalysts,<sup>4</sup> sensors,<sup>5</sup> and superconductors.<sup>6</sup> Meanwhile, ZnO is a well-known n-type semiconductor ( $E_g = 3.37 \text{ eV}$  at 300 K) with high electron mobility and low recombination loss,<sup>7</sup> and widely used in optoelectronics,<sup>8</sup> gas sensing,<sup>9,10</sup> catalysis,<sup>11</sup> and solar cell.<sup>12</sup> A number of methods such as chemical vapor deposition,<sup>12</sup> thermal evaporation,<sup>11,13,14</sup> template methods,<sup>15</sup> and hydrothermal technique<sup>16</sup> have been developed to synthesize nanostructured CuO and/or ZnO materials. Recently, it has been reported that ZnO/CuO composites with p-n heterojunction structures exhibited improved performance in photocatalysis,<sup>3,7</sup> chemical and humidity sensing,<sup>10</sup> environmental pollution abatement,<sup>17</sup> self-cleaning sensor,<sup>18</sup> and selective H<sub>2</sub>S detection.<sup>19</sup> As a result, many ZnO/CuO composite nanostructures have been fabricated, including CuO/ZnO core/shell heterostructured nanowires prepared by thermal

decomposition,<sup>2</sup> flower-like CuO-ZnO heterostructured nanowires by chemical and photochemical deposition,<sup>3</sup> CuO-ZnO hollow spheres by using highly uniformly monodispersed Cu-embedded carbon spheres as templates under hydrothermal conditions,<sup>7</sup> corn-like CuO-ZnO structures by hydrothermal and photo-deposition,<sup>10</sup> Cu-ZnO nanocrystallites by aqueous thermolysis,<sup>13</sup> CuO/ZnO nanocorals by hydrothermal process,<sup>20</sup> ZnO/CuO nanotrees by hydrothermal method combined with thermal oxidation on Cu substrates,<sup>18</sup> and CuO-ZnO wire-dots by photochemical precipitation.<sup>3</sup> However, it remains a great challenge to create hierarchically structured CuO/ZnO with a regular size and morphology.

As we know, methylchlorosilanes (MCSs) are commercially synthesized *via* the Rochow reaction discovered in 1940s,<sup>21</sup> in which, solid silicon (Si) reacts with gaseous methyl chloride (MeCl) in the presence of Cu-based catalysts physically mixed with trace promoters<sup>21,22</sup> to produce MCSs including methyltrichlorosilane (CH<sub>3</sub>SiCl<sub>3</sub>, M1), dimethyldichlorosilane ((CH<sub>3</sub>)<sub>2</sub>SiCl<sub>2</sub>, M2), trimethylchlorosilane ((CH<sub>3</sub>)<sub>3</sub>SiCl, M3), and other trace Si-containing compounds.<sup>23</sup> Among these MCSs, M2 is the most desirable monomer used for the production of silicone polymers in organosilane industry.<sup>24</sup> Generally, the M2 selectivity in the Rochow reaction is highly dependent on the Cu-based catalysts, such as metallic Cu<sup>25</sup> and Cu compounds (Cu<sub>2</sub>O,<sup>26</sup> CuO,<sup>27</sup> CuCl,<sup>28</sup> and Cu-Cu<sub>2</sub>O-CuO composite<sup>29</sup>). However, the catalytic mechanism is not fully understood.<sup>30</sup> On the other hand, Zn or ZnO as Zn-based promoter additives also play an important role in this

<sup>a</sup>College of Chemical and Environmental Engineering, Qingdao University, Qingdao, China 266071. E-mail: xlshe@126.com; fbsu@mail.ipe.ac.cn;

Fax: +86-10-82544851; Tel: +86-10-82544850

<sup>b</sup>State Key Laboratory of Multiphase Complex Systems, Institute of Process Engineering, Chinese Academy of Sciences, Beijing, China 100190.

E-mail: wangyl@mail.ipe.ac.cn

<sup>c</sup>Institute of Chemical Engineering and Sciences, A\*star, 1 Pesek Road, Jurong Island, Singapore 627833

† Electronic supplementary information (ESI) available. See DOI: 10.1039/c3ra00171g

reaction,<sup>31-33</sup> but their promotion mechanism is still not clear yet. The commercially used Cu catalysts always have dense structures, irregular morphologies and are in micrometer sizes. Thus, it is necessary to explore above complex gas-solid-solid phase reaction using defined CuO–ZnO composites as active Cu/Zn-based catalysts with specific morphology and designed structures.

Herein, we present a simple solvothermal method to rationally grow flower-like ZnO on urchin-like CuO (f-ZnO@u-CuO) microspheres forming a novel hierarchical composite as the model Cu/Zn-based catalysts for the Rochow reaction. A possible formation mechanism is proposed based on the observation of a series of reaction intermediates. Compared to the Cu-based catalysts physically mixed with ZnO promoter, the obtained f-ZnO@u-CuO microspheres show better catalytic properties for M2 synthesis because of the stronger synergistic effect between CuO and ZnO.

## 2. Experimental

### 2.1. Material synthesis

All chemicals, including copper nitrate trihydrate ( $\text{Cu}(\text{NO}_3)_2 \cdot 3\text{H}_2\text{O}$ , A.R., 99%), zinc nitrate hexahydrate ( $\text{Zn}(\text{NO}_3)_2 \cdot 6\text{H}_2\text{O}$ , AR, 99%), ethanol ( $\text{CH}_3\text{CH}_2\text{OH}$ , A.R., 99%), ammonia solution ( $\text{NH}_4\text{OH}$ , A.R., 25–28%), sodium hydroxide ( $\text{NaOH}$ , A.R., 99%), sodium nitrate ( $\text{NaNO}_3$ , A.R., 99%), copper oxide (CuO, A.R., 99%, denoted c-CuO in this work), and zinc oxide (ZnO, A.R., 99%, denoted c-ZnO) were purchased from Sinopharm Chemical Reagent Co. Ltd., Shanghai, China, and used without further purification.

All the samples were synthesized by a solvothermal method,<sup>27,34</sup> and the synthetic conditions such as hydrothermal temperature, reaction time, the amount of chemicals used in this work are compiled in Table 1. In a typical synthesis (e.g. sample Z3 in Table 1), 0.5 g  $\text{Cu}(\text{NO}_3)_2 \cdot 3\text{H}_2\text{O}$  and 0.6 g

$\text{Zn}(\text{NO}_3)_2 \cdot 6\text{H}_2\text{O}$  were dissolved in 50.0 mL  $\text{CH}_3\text{CH}_2\text{OH}$ , and then 30.0 mL  $\text{NH}_4\text{OH}$ , 10.0 mL NaOH solution (1.0 M) and 2.0 g  $\text{NaNO}_3$  were added to form a solution. After stirred for 10 min, the solution was transferred into a stainless steel autoclave with a Teflon-lined chamber, and the autoclave was heated to 130 °C and maintained for 18 h. After cooled to room temperature in air, the solid sample was filtrated, washed with distilled water and ethanol several times, and dried under vacuum at 60 °C for 6 h.

### 2.2. Characterization

X-ray diffraction (XRD) patterns were recorded on a PANalytica X'Pert PRO MPD using the Cu-K $\alpha$  radiation ( $\lambda = 1.5418 \text{ \AA}$ ). The crystal size of the products was calculated using the Debye-Scherrer equation. The microscopic features were observed by field-emission scanning electron microscopy (SEM) (JSM-6700F, JEOL, Tokyo, Japan) and transmission electron microscopy (TEM) (JEM-2010F, JEOL, Tokyo, Japan). The compositional analysis was performed with energy-dispersive X-ray (EDX) spectroscopy (Shimadzu). The chemical composition was determined by X-ray photoelectron spectroscopy (XPS) (Model VG ESCALAB 250 spectrometer, Thermo Electron, U.K.) using a nonmonochromatized Al-K $\alpha$  X-ray source (1486.6 eV). The elemental analysis was carried out with Inductively Coupled Plasma Optical Emission Spectrometer (ICP-OES) (Optima 5300DV, perkin Elmer, American). The temperature-programmed reduction (TPR) measurements were carried out on Automated Chemisorption Analyzer (chemBET pulsar TPR/TPD, Quantachrome). 0.10 g sample loaded into a quartz U-tube was first degassed at 300 °C for 60 min under helium. After the temperature was cooled to 30 °C, the gas was changed to 9.91%  $\text{H}_2$ -Ar (30 mL  $\text{min}^{-1}$ ) and subsequently heated up to 1100 °C at 10 °C  $\text{min}^{-1}$ . The porous nature of the samples was investigated using physical adsorption of  $\text{N}_2$  at  $-196 \text{ }^\circ\text{C}$  on an automatic volumetric sorption analyzer (NOVA3200e, Quantachrome). Prior to the measurement, the sample was degassed at 200 °C for 5 h under vacuum. The specific surface

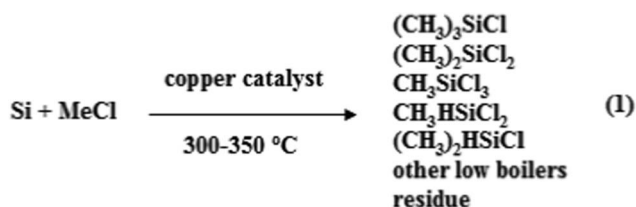
**Table 1** The synthesis conditions used in the sample preparation

Sample	Copper nitrate (g)	Zinc nitrate (g)	Ethanol (mL)	Ammonia water (mL)	Sodium hydroxide (mL)	Sodium nitrate (g)	Temperature (°C)	Time (h)
Z0	1.0	0	50.0	30.0	10.0	5.0	180	18
Z1	0.5	0.6	50.0	30.0	10.0	2.0	80	18
Z2	0.5	0.6	50.0	30.0	10.0	2.0	100	18
Z3	0.5	0.6	50.0	30.0	10.0	2.0	130	18
Z4	0.5	0.6	50.0	30.0	10.0	2.0	150	18
Z5	0.5	0.6	50.0	30.0	10.0	2.0	130	0.4
Z6	0.5	0.6	50.0	30.0	10.0	2.0	130	0.5
Z7	0.5	0.6	50.0	30.0	10.0	2.0	130	2
Z8	0.5	0.6	50.0	30.0	10.0	2.0	130	30
Z9	0.5	0.6	50.0	30.0	10.0	1.0	130	18
Z10	0.5	0.6	50.0	30.0	10.0	3.0	130	18
Z11	0.5	0.6	50.0	30.0	10.0	4.0	130	18
Z12	0.5	0.6	50.0	5.0	13.5	2.0	130	18
Z13	0.5	0.6	50.0	10.0	13.5	2.0	130	18
Z14	0.5	0.6	50.0	15.0	13.5	2.0	130	18
Z15	0.5	0.6	50.0	20.0	13.5	2.0	130	18
Z16	0.5	0.6	50.0	25.0	13.5	2.0	130	18
Z17	0.5	0.6	50.0	30.0	13.5	2.0	130	18

areas were determined according to the Brunauer–Emmett–Teller (BET) method in the relative pressure range of 0.05–0.2.

### 2.3. Catalytic measurement

The evaluation of catalyst performance was carried out with a typical MCS lab fixed-bed reactor.<sup>35</sup> 5.0 g of Si powder (20–50 mesh, provided by Jiangsu Hongda New Material Co., Ltd. the impurity level of other elements was listed in Table S1, ESI†) were homogeneously mixed with 0.5 g obtained sample as Cu-based catalyst to form a contact mass. The reactor system was initially purged with purified N<sub>2</sub> for 0.5 h followed by heating to 325 °C within 1 h under N<sub>2</sub> (12.5 mL min<sup>-1</sup>). Subsequently, N<sub>2</sub> was turned off and gas MeCl (12.5 mL min<sup>-1</sup>) was introduced into the reactor. After a given period reaction of 24 h at 325 °C, the reaction was terminated. The gas products were cooled down to liquid phase using a water circulating bath controlled at 5 °C by a programmable thermal circulator (GDH series, Ningbo xinzhì biological technology Co., LTD). The products in the liquid solution were quantitatively analyzed on a Gas Chromatograph (GC) (Agilent Technologies GC-7890A) equipped with KB-201 column (60 m) and TCD detector. The compositions of the reaction products were analyzed by the peak area ratio (in percentage).<sup>36</sup> The products, which mainly contained M1, M2, M3, methylchlorosilane (CH<sub>3</sub>SiHCl<sub>2</sub>, M4), dimethylchlorosilane ((CH<sub>3</sub>)<sub>2</sub>SiHCl, M5), low-boiling residue (M6), and high-boiling residue (M7), were identified with gas chromatography-mass spectrometry (GC-MS) (QP2010, Shimadzu).<sup>37</sup> The Rochow reaction is shown in the following formula 1:



The spent contact mass (residual solid after reaction) containing unreacted Si powder, Cu compounds, and promoters were weighed to calculate Si conversion ( $C_{\text{Si}}$ ) according to the following formula:<sup>37</sup>

$$\text{Conversion of Si } (C_{\text{Si}}) = \frac{\text{weight}_{\text{contact mass before reaction}} - \text{weight}_{\text{contact mass after reaction}}}{\text{weight}_{\text{Si before reaction}}} \times 100\% \quad (2)$$

## 3. Results and discussion

### 3.1. Characterization of synthesized materials

Since the morphology and structure of CuO and/or ZnO are highly dependent on the synthesis conditions,<sup>27,32</sup> we systematically investigated the effect of the solvothermal temperature (Fig. S1, ESI†), time (Fig. S2, ESI†), amount of mineralization agent (sodium nitrate) (Fig. S3, ESI†) and ammonia (Fig. S4, ESI†) added. Several representative samples were selected for further characterization, including Z0 (urchin-like CuO,

denoted u-CuO), Z3 (flower-like ZnO grown on urchin-like CuO, denoted f-ZnO@u-CuO), Z7 (flower-like ZnO partially grown on urchin-like CuO, denoted f-ZnO/@u-CuO), and Z8 (flower-like ZnO mixed with urchin-like CuO, denoted f-ZnO/u-CuO).

Fig. 1a shows the SEM image of u-CuO. It is seen that the u-CuO microspheres in a size of 2–6 μm are assembled by nanoplates in a size of several tens of nanometres (inset of Fig. 1a). For f-ZnO/u-CuO shown in Fig. 1b, the u-CuO and f-ZnO phases are separated, in which, the average diameter of u-CuO microspheres is 6 μm, which are assembled by CuO nanorods with an average cross-section diameter of 100 nm (inset of Fig. 1b), while the f-ZnO flowers are also assembled by nanorods with average cross-section diameter and length of 400 nm and 3.0 μm, respectively. Fig. 1c shows the SEM image of f-ZnO/@u-CuO, in which, f-ZnO flowers are partially grown on the u-CuO microspheres surface. For f-ZnO@u-CuO, its SEM image (Fig. 1d) shows the f-ZnO flowers are grown out from the surface of u-CuO microspheres. The size of this hierarchical structure is about 3–8 μm. The yield of f-ZnO@u-CuO is about 66.7 wt%. These results suggest that the defined morphology and specific structure of CuO and/or ZnO microspheres can be obtained under different synthesis conditions. Fig. 1e shows the high magnification SEM image of the f-ZnO@u-CuO sample. It is clearly seen that f-ZnO covers on the surface of u-CuO, further confirmed by EDX analysis shown in Fig. 1e-A and 1e-B, in which, the atomic ratio of Cu to O is around 1.0 : 1.0, close to the stoichiometric ratio of 1.0 : 1.0 for CuO in Fig. 1e-A, and the atomic ratio of Zn to O is 0.9 : 1.0, close to the stoichiometric ratio of 1.0 : 1.0 for ZnO in Fig. 1e-B. The surface areas of these Cu/Zn-based catalysts compiled in Table 2 are 5.1 m<sup>2</sup> g<sup>-1</sup> for c-ZnO + c-CuO, 12.4 m<sup>2</sup> g<sup>-1</sup> for c-ZnO + u-CuO, 14.1 m<sup>2</sup> g<sup>-1</sup> for f-ZnO/u-CuO, 20.6 m<sup>2</sup> g<sup>-1</sup> for f-ZnO/@u-CuO, and 22.7 m<sup>2</sup> g<sup>-1</sup> for f-ZnO@u-CuO.

Fig. 2 shows the XPS spectra of the f-ZnO@u-CuO sample. The wide XPS spectrum in Fig. 2a confirms the presence of Zn, Cu, O, and C elements. Fig. 2b shows the Cu 2p spectrum, in which, the characteristic intense peaks of Cu 2p are centered at the binding energy (BE) of 934.3 eV (Cu 2p<sub>3/2</sub>) and 953.7 eV (Cu 2p<sub>1/2</sub>), and the BE gap between Cu 2p<sub>3/2</sub> and Cu 2p<sub>1/2</sub> is approximately 20 eV, suggesting that the divalent state of Cu in

the form of CuO on the surface of f-ZnO@u-CuO sample.<sup>38</sup> Fig. 2c shows the Zn 2p spectrum. It is seen that there are two characteristic peaks located at BE of 1020.8 eV (Zn 2p<sub>3/2</sub>) and 1043.9 eV (Zn 2p<sub>1/2</sub>). The BE gap between Zn 2p<sub>3/2</sub> and Zn 2p<sub>1/2</sub> is about 23 eV, indicating that the oxidation state of Zn is + 2 in f-ZnO@u-CuO sample.<sup>39</sup> Particularly, the first BE shows a negative shift compared with the Zn 2p<sub>3/2</sub> (1022.0 eV) of pure ZnO, possibly ascribed to the interaction between u-CuO and f-ZnO.<sup>40</sup> Moreover, the Cu : Zn atomic ratio derived from their spectra is around 1.0 : 1.0, consistent with that of metal precursors used, which is further confirmed by ICP-OES analysis, suggesting the molar ratio of ZnO : CuO is 1.0 : 1.0

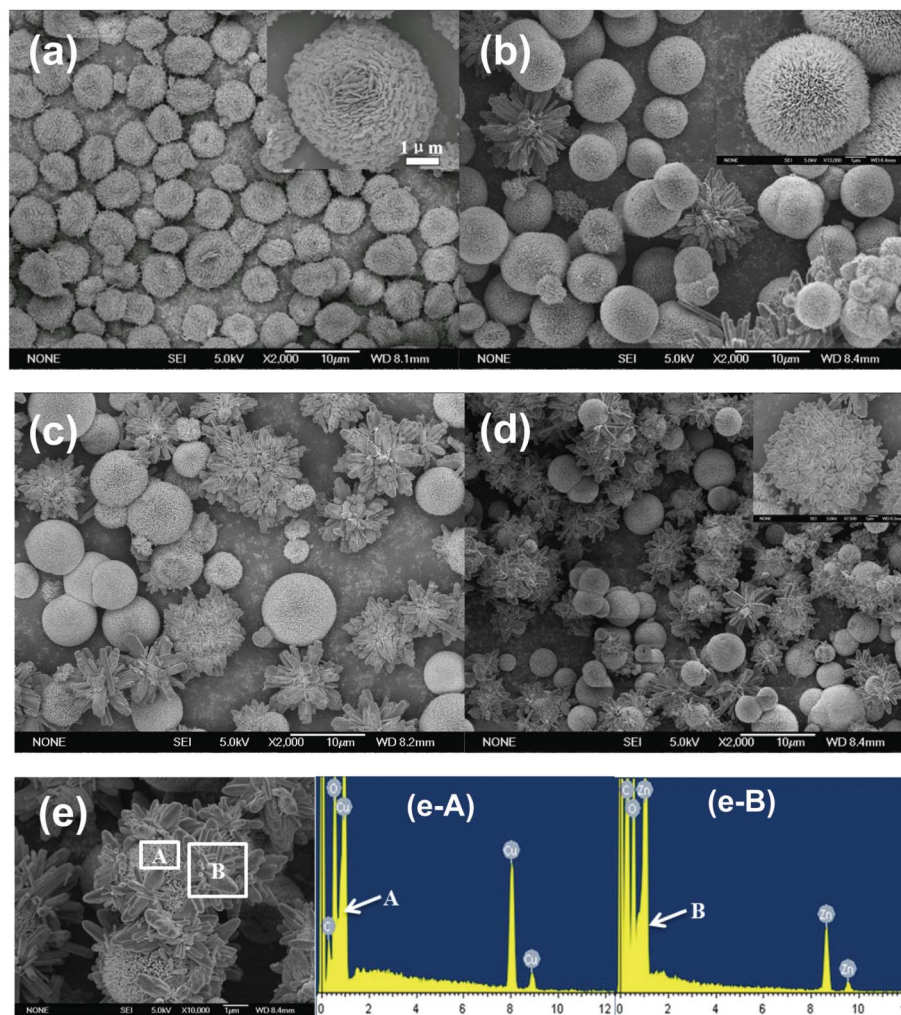


**Fig. 1** SEM images of the samples: (a) u-CuO, (b) f-ZnO/u-CuO, (c) f-ZnO/@u-CuO, and (d) f-ZnO@u-CuO, together with (e-A) EDS spectra focusing on the A zone in (e) and (e-B) EDS spectra focusing on the B zone in (e).

for the f-ZnO@u-CuO sample. For other samples of f-ZnO/u-CuO and f-ZnO/@u-CuO, this ratio obtained by ICP-OES is also about 1.0 : 1.0.

Fig. 3a shows the TEM image of f-ZnO@u-CuO, in which f-ZnO flowers are grown on the surface of the u-CuO micro-

spheres. The high resolution TRM (HRTEM) image in Fig. 3b presents the lattice structure of ZnO and CuO. The lattice distance of the two parts (I and II) is 0.20 nm and 0.22 nm, in good agreement with the (−111) lattice plane of monoclinic CuO and the (101) lattice plane of hexagonal ZnO, respectively. The TEM and HRTEM results demonstrate that the microsphere is a composite containing both CuO and ZnO phases, and f-ZnO is a single crystalline with [0001] as the preferential growth direction. It is well known that composite structures can form easily when the crystal planes of the two different materials have a close inter-plane spacing and similar crystal structures.<sup>41</sup> In the above microspheres, CuO has a monoclinic structure and ZnO has a hexagonal structure, and the CuO (−111) and ZnO (101) planes have a similar inter-plane spacing (0.20 vs. 0.22 nm), thus the composite CuO–ZnO structure can form easily.

### 3.2. Formation mechanism of f-ZnO@u-CuO

The possible reactions during the synthesis process are expressed as following equations (Eq.):

**Table 2** The crystal sizes, H<sub>2</sub>-TPR parameters, and surface areas of all the catalysts

Sample	$d_{\text{CuO}}^a$ (nm)	$d_{\text{ZnO}}^a$ (nm)	$T_{\text{TPR}}^b$ (°C)	$T_{\text{M}}^c$ (°C)	$S_{\text{BET}}^d$ (m <sup>2</sup> g <sup>−1</sup> )
u-CuO	26.1	0.0	270–380	331	9.8
c-ZnO + c-CuO	30.2	50.9	300–420	348	5.1
c-ZnO + u-CuO	28.2	50.9	220–310	270	12.4
f-ZnO/u-CuO	28.2	43.5	200–290	241	14.1
f-ZnO/@u-CuO	26.2	42.5	150–250	221	20.6
f-ZnO@u-CuO	25.1	41.4	140–230	210	22.7

<sup>a</sup> The crystal size of CuO and ZnO calculated from the XRD patterns.

<sup>b</sup> Reduction temperature range of samples. <sup>c</sup> Temperatures at the peak maximum. <sup>d</sup> The BET surface area of the catalysts.

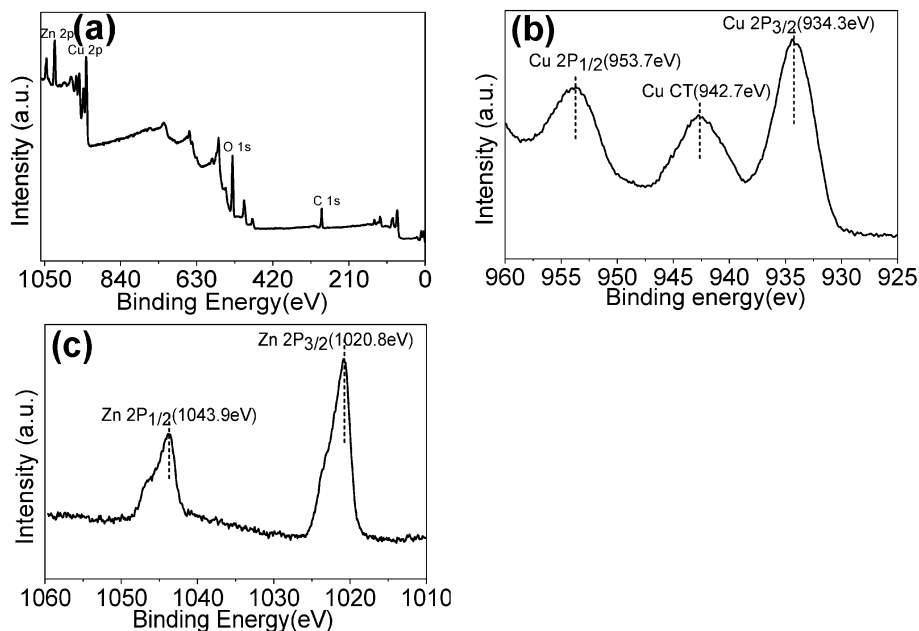
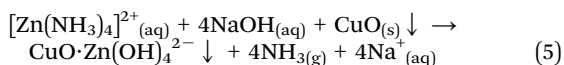
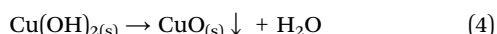
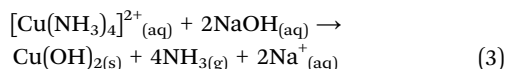
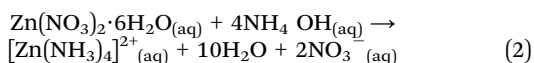
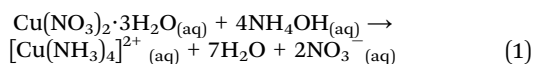


Fig. 2 XPS spectra of the sample f-ZnO@u-CuO: (a) wide spectrum, (b) Cu 2p spectrum, and (c) Zn 2p spectrum.



The growth mechanism of f-ZnO@u-CuO is illustrated in Fig. 4. Firstly,  $\text{Cu}(\text{NO}_3)_2 \cdot 3\text{H}_2\text{O}$  and  $\text{Zn}(\text{NO}_3)_2 \cdot 6\text{H}_2\text{O}$  are dissolved in ammonia solution to form  $[\text{Cu}(\text{NH}_3)_4]^{2+}$  and  $[\text{Zn}(\text{NH}_3)_4]^{2+}$  (eqn (1) and (2)), respectively.<sup>10</sup> The reaction constants of  $\text{Cu}(\text{OH})_2$  and  $\text{Zn}(\text{OH})_2$  at 25 °C are  $4.8 \times 10^{-20}$

and  $1.8 \times 10^{-14}$ , as the precipitation pH value ranges of  $\text{Cu}(\text{OH})_2$  and  $\text{Zn}(\text{OH})_2$  are 3.9–7.3 and 7.4–11.8 respectively. After adding NaOH,  $[\text{Cu}(\text{NH}_3)_4]^{2+}$  species firstly react with NaOH to form intermediate  $\text{Cu}(\text{OH})_2$  in autoclave at the high temperature (eqn (3)).<sup>42</sup> With the increase of reaction time (25 min), u-CuO crystal nucleus are generated *via* the decomposition of  $\text{Cu}(\text{OH})_2$  (eqn (4)),<sup>43</sup> and subsequently the u-CuO microspheres (Fig. S2a, ESI†) are obtained *via* Ostwald ripening,<sup>44,45</sup> as shown in Fig. 4. Because of the high concentration of  $[\text{Zn}(\text{NH}_3)_4]^{2+}$  in the solution, nucleation and growth of ZnO will take place surrounding the created CuO crystals *via* the Ostwald ripening,<sup>44,46</sup> owing to the lower activation energy barrier of heterogeneous nucleation. Thus,  $\text{CuO} \cdot \text{Zn}(\text{OH})_4^{2-}$  intermediate is obtained from  $[\text{Zn}(\text{NH}_3)_4]^{2+}$  species, which get rid of complexation on u-CuO microcrystal (eqn (5)). With the reaction time increasing to 30 min, f-ZnO nanorods are aligned perpendicularly to the u-CuO spherical surface, but along the main crystallographic axes of CuO and pointed to a common center, *via* the so-called “oriented attachment” process (Fig. S2b, ESI† and eqn (6)),<sup>47</sup> which is shown in the Fig. 4. Finally, after the 18 h reaction, the growth of f-ZnO on u-CuO is completed forming the f-ZnO@u-CuO (Fig. S2d, ESI†).

### 3.3. Characterization of the Cu/Zn-based catalysts

To investigate the catalytic activity of these Cu/Zn-based catalysts for Rochow reaction, we characterized some representative samples with the same molar ratio of CuO and ZnO (1.0 : 1.0), including physically mixed commercial ZnO and CuO (denoted c-ZnO + c-CuO) (their SEM images, XRD patterns and  $\text{H}_2$ -TPR curves are shown in Fig. S5, ESI†), physically mixed c-ZnO and u-CuO (denoted c-ZnO + u-CuO), f-ZnO/u-CuO, f-ZnO/@u-CuO, and f-ZnO@u-CuO. Fig. 5a shows their XRD patterns together with u-CuO as a compar-

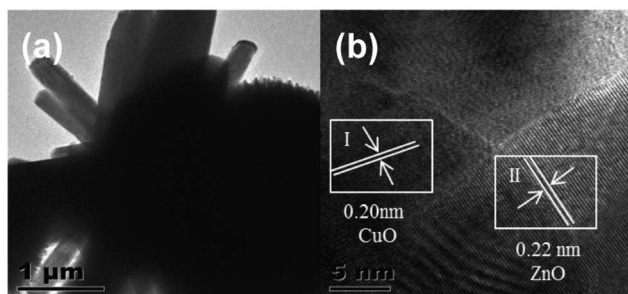


Fig. 3 TEM (a) and HRTEM (b) images of f-ZnO@u-CuO.

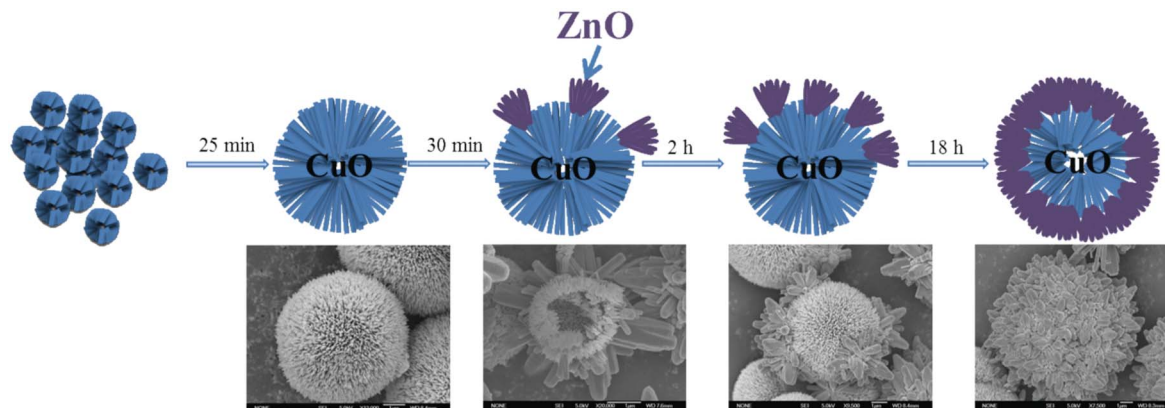


Fig. 4 Schematic illustration of the f-ZnO@u-CuO growth process.

ison. The diffraction peaks of all the samples can be readily indexed to a monoclinic CuO (JCPDS: 65-2309) and a hexagonal wurtzite ZnO (JCPDS: 36-1451). The crystal sizes of CuO and ZnO are calculated based on the  $2\theta$  values of  $35.8^\circ$  and  $36.4^\circ$  respectively and shown in Table 2, which are in the similar size level of 20–30 nm for CuO and 41–51 nm for ZnO. Fig. 5b shows their enlarged view in the  $2\theta$  angle range of  $34\text{--}37^\circ$ , in which, a characteristic blue shift is observed for f-ZnO/@u-CuO and f-ZnO@u-CuO. Both the (–111) diffraction peak of CuO and (101) diffraction peak of ZnO move to lower angle region, implying the partial merging of the lattices of CuO (–111) and ZnO (101) due to the interaction of crystal surface.<sup>48</sup> As a result, the p-n heterojunctions are formed between the lattices of CuO and ZnO.

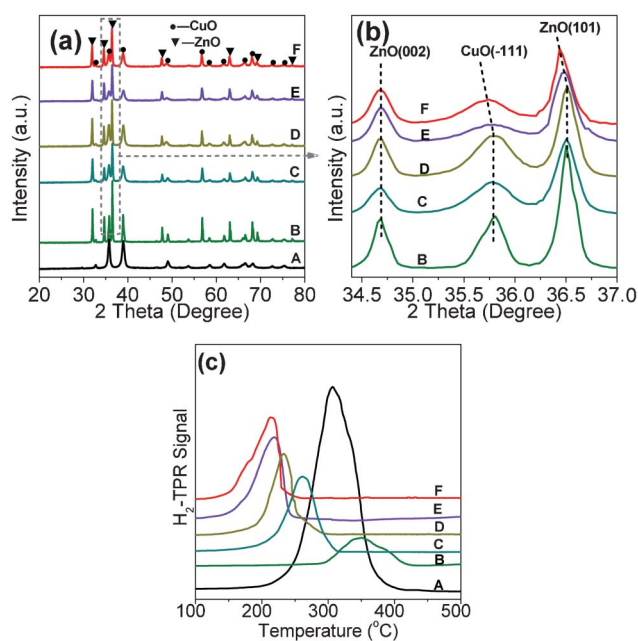


Fig. 5 XRD patterns (a), enlarged view in the  $2\theta$  angle range of  $34\text{--}37^\circ$  (b), and  $\text{H}_2$ -TPR curves (c) of all the samples (A: u-CuO, B: c-ZnO + c-CuO, C: c-ZnO + u-CuO, D: f-ZnO/u-CuO, E: f-ZnO/@u-CuO, and F: f-ZnO@u-CuO).

Fig. 5c shows the  $\text{H}_2$ -TPR profiles of all the catalysts. As a comparison, the TPR curve of u-CuO is shown at the bottom of the graph. All the Cu/Zn-based catalysts display one reduction peak but they are localized at different temperature ranges. The peak temperatures ( $T_M$ ) are compiled in Table 2. Although the average CuO crystal size in all the catalysts is in a similar level, the order of  $T_M$  for all the Cu/Zn-based catalysts is c-ZnO + c-CuO ( $348^\circ\text{C}$ ) > c-ZnO + u-CuO ( $270^\circ\text{C}$ ) > f-ZnO/u-CuO ( $241^\circ\text{C}$ ) > f-ZnO/@u-CuO ( $221^\circ\text{C}$ ) > f-ZnO@u-CuO ( $210^\circ\text{C}$ ), suggesting that ZnO is able to promote the reduction of CuO possibly because the regular morphology and small particle size of CuO or ZnO have lower reaction activation energy than the commercial CuO or ZnO.<sup>32</sup> More importantly, f-ZnO@u-CuO is formed by well-dispersed CuO and ZnO particles with the intimate contact to each other<sup>49</sup> and the well-developed p-n heterojunction structure leading to a closer electrical contact between ZnO and CuO particles with a consequent coupling of their Fermi levels and probably promoting the copper reduction.<sup>50</sup> This idea has indeed been supported by the XPS studies of these samples. Therefore, an enhanced synergistic effect due to the stronger interaction of crystal surfaces in f-ZnO@u-CuO is convincible,<sup>50</sup> as evidenced by the weakening of the Cu–O bond. Also, the peak area of these Cu/Zn-based catalysts is about half of that of u-CuO because the molar ratio of ZnO : CuO is approximately 1.0 : 1.0 in all Cu/Zn-based catalysts.

Table 3 Catalytic performance of all the Cu/Zn-based catalysts for the Rochow reaction

Sample	Product selectivity (%)							C-Si (%)
	M1	M2	M3	M4	M5	M6	M7	
c-ZnO + c-CuO	25.9	42.9	2.7	0.8	0.0	0.0	27.7	4.8
c-ZnO + u-CuO	14.2	46.4	2.2	0.3	0.7	3.5	32.7	10.8
f-ZnO/u-CuO	18.6	49.5	1.5	8.0	0.4	2.5	19.5	10.4
f-ZnO/@u-CuO	22.9	60.5	2.1	11.2	0.5	1.6	1.2	18.2
f-ZnO@u-CuO	18.0	69.6	1.6	5.5	0.6	3.2	1.5	20.0
f-ZnO@u-CuO <sup>a</sup>	21.7	68.6	1.7	3.2	0.2	0.7	3.9	20.2

<sup>a</sup> Repeated testing.

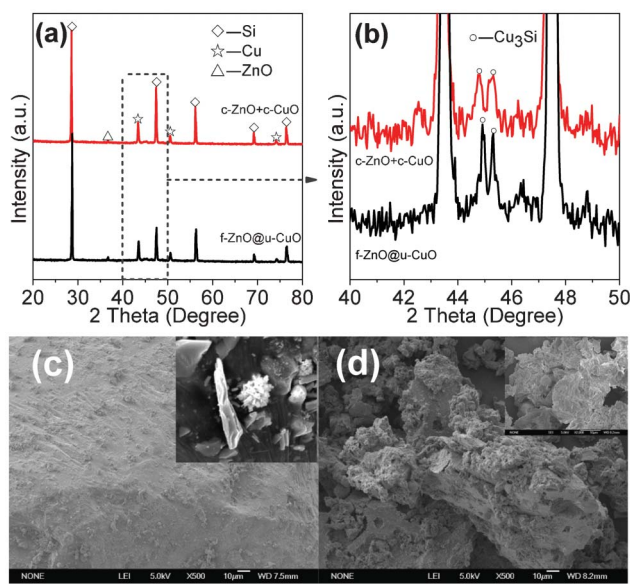
### 3.4 Catalytic property

Table 3 shows the catalytic performance of all the catalysts for M<sub>2</sub> synthesis *via* the Rochow reaction. On the physically mixed c-ZnO + c-CuO catalyst, 42.9% of M<sub>2</sub> selectivity and 4.8% of Si conversion are obtained. For c-ZnO + u-CuO catalyst, the M<sub>2</sub> selectivity and Si conversion rise up to 46.4% and 10.8%, respectively, and those of f-ZnO/u-CuO are similar to those of c-ZnO + u-CuO. For f-ZnO/@u-CuO catalyst, the observed M<sub>2</sub> selectivity (60.5%) and Si conversions (18.2%) are much higher than those of c-ZnO + c-CuO, c-ZnO + u-CuO, and f-ZnO/u-CuO. More importantly, the f-ZnO/@u-CuO catalyst shows the highest M<sub>2</sub> selectivity of 69.6% and the highest Si conversions of 20.0% among all the catalysts, which is further confirmed by the repeated testing.

As M<sub>2</sub> is the most valuable monomer precursor in organosilane industry, the Rochow reaction is carried out industrially to maximize the selectivity for M<sub>2</sub>. The above results demonstrate that the f-ZnO/@u-CuO shows much higher M<sub>2</sub> selectivity and Si conversion than the others. In the Rochow reaction, the intermetallic phase of Cu<sub>3</sub>Si is considered to be the major active intermediate phase.<sup>51,52</sup> It is believed that at the beginning of the reaction, Cu atoms, which are essentially mobile in the reaction system,<sup>22</sup> firstly diffuse on and into Si surface to form the active alloying Cu<sub>3</sub>Si species at the interface of Cu and Si.<sup>23,53,54</sup> These species are the precondition of the synthesis reaction, which play an important role in guiding the reactant-catalyst interaction towards a higher specificity of the reaction.<sup>53,55</sup> Meanwhile, promoter additives such as Zn, ZnO, and Sn are of importance in improving the catalytic performance,<sup>29,33,56,57</sup> which could decrease the segregation energy of Si and promote the crystal growth of Cu silicides. Fig. 6a shows the XRD patterns of the contact masses (f-ZnO/@u-CuO + Si and c-ZnO + c-CuO + Si)

after the reaction. It can be seen that, after the reaction, the contact masses are composed of Si, Cu, and ZnO, but no CuO species, probably due to the reaction of chlorosilane with the lattice oxygen from CuO.<sup>26</sup> As a promoter, ZnO remains unchanged in the reaction. The enlarged view in Fig. 6b shows the presence of Cu<sub>3</sub>Si species in the two contact masses. Although the intensity of Cu peaks for both contact masses are very similar, a much higher intensity of Cu<sub>3</sub>Si is observed in f-ZnO/@u-CuO + Si, implying that the f-ZnO/@u-CuO catalyst is more active in creating Cu<sub>3</sub>Si than c-ZnO + c-CuO. This may be due to that the stronger synergistic effect existing in this catalyst with a p-n heterojunction structure between the CuO and ZnO in f-ZnO/@u-CuO lowering the activation energy although this synergistic effect is not fully understood yet at the moment. The SEM images of the contact masses before the reaction in Fig. 6c show that the Si surface was smooth and dense with uniformly distributed f-ZnO/@u-CuO (insert of Fig. 6c). After the reaction, the Si surface became coarse or porous (Fig. 6d), indicating that the f-ZnO/@u-CuO catalyst could “drills” the Si surface during the reaction and gradually invaded into its interior. Therefore, the Cu-based catalyst bonded tightly with the ZnO promoter should be significant for the Rochow reaction.

Despite the fact that f-ZnO/@u-CuO shows a relatively higher M<sub>2</sub> selectivity and Si conversion than the others, it should be mentioned that the content of ZnO in f-ZnO/@u-CuO is higher than that of the commercially used (normally less than 10 wt% of Cu content).<sup>58</sup> However, our intension in this work is to explore the importance of the synergistic effect between CuO and ZnO in the Rochow reaction. It has been proved that, by carefully design a Cu/Zn-based catalyst with a specific morphology, the synergistic function between CuO and ZnO can be significantly enhanced, thus improving its catalytic performance. As we know, many Cu compounds such as metallic Cu<sup>25</sup> and Cu compounds (Cu<sub>2</sub>O,<sup>26</sup> CuO,<sup>27</sup> CuCl,<sup>28</sup> and Cu-Cu<sub>2</sub>O-CuO composite<sup>29</sup>) are active for the Rochow reaction, and thus along this way, the incorporation of promoters such as Zn<sup>31</sup> and ZnO<sup>32</sup> within these Cu compounds to form numerous novel Cu/Zn-based nanocomposites may pave a way to find the highly efficient catalysts for M<sub>2</sub> synthesis. In addition, the nanostructured CuO/ZnO composites with a well-developed p-n heterojunction structure at the CuO and ZnO interfaces may be used as photocatalysts for the degradation of dye contaminants,<sup>17</sup> photoelectrodes for H<sub>2</sub> generation,<sup>2</sup> humidity sensor,<sup>20</sup> superhydrophobic materials,<sup>18</sup> and photocatalysts for H<sub>2</sub> generation.<sup>38</sup>



**Fig. 6** XRD patterns of contact masses (f-ZnO/@u-CuO + Si and c-ZnO + c-CuO + Si) after reaction (a) and enlarged view in the 2θ angle range of 40–50° (b), SEM images of contact masses (f-ZnO/@u-CuO + Si) before (c) and after (d) reaction.

## 4. Conclusions

In summary, we have demonstrated the growth of the flower-like ZnO on the urchin-like CuO (f-ZnO/@u-CuO) microspheres, and their improved catalytic function in dimethyldichlorosilane synthesis. Compared to the physically mixed CuO and ZnO catalysts, the f-ZnO/@u-CuO catalyst exhibits higher M<sub>2</sub> selectivity and Si conversion. This is because the strong synergistic effect of the p-n heterojunction formed at the interfaces between CuO and ZnO. This works demonstrates

the possibility that a proper morphology variation is conducive to the catalytic synthesis of dimethyldichlorosilane *via* the Rochow reaction.

## Acknowledgements

The authors gratefully acknowledge the financial supports from the National Natural Science Foundation of China (No. 21206172 and 51272252), Hundred Talents Program of the Chinese Academy of Sciences (CAS), CAS-Locality Cooperation Program (No. DBNJ-2011-058), State Key Laboratory of Multiphase Complex Systems (No. MPC-2011-D-14), and National Youth Foundation of China (No. 50903045).

## References

- C. Wang, Y. Ye, B. Tao and B. Geng, *CrystEngComm*, 2012, **14**, 3677–3684.
- X. Zhao, P. Wang and B. Li, *Chem. Commun.*, 2010, **46**, 6768–6770.
- S. Jung and K. Yong, *Chem. Commun.*, 2011, **47**, 2643–2645.
- Y. Feng and X. Zheng, *Nano Lett.*, 2010, **10**, 4762–4766.
- J. Zhang, J. Liu, Q. Peng, X. Wang and Y. Li, *Chem. Mater.*, 2006, **18**, 867–871.
- S. Manna, K. Das and S. K. De, *ACS Appl. Mater. Interfaces*, 2010, **2**, 1536–1542.
- X. Shi, X. Yang, X. Gu and H. Su, *J. Solid State Chem.*, 2012, **186**, 76–80.
- R. Zhang, L. Fan, Y. Fang and S. Yang, *J. Mater. Chem.*, 2008, **18**, 4964–4970.
- J. H. Kim and K. J. Yong, *J. Phys. Chem. C*, 2011, **115**, 7218–7224.
- M. M. Rahman, A. Jamal, S. B. Khan and M. Faisal, *ACS Appl. Mater. Interfaces*, 2011, **3**, 1346–1351.
- Z. Liu, Z. Jin, W. Li and J. Qiu, *Mater. Res. Bull.*, 2006, **41**, 119–127.
- C. K. Xu, P. Shin, L. L. Cao and D. Gao, *J. Phys. Chem. C*, 2010, **114**, 125–129.
- S. N. Rishikeshi and S. Joshi, *J. Therm. Anal. Calorim.*, 2012, **109**, 1473–1479.
- Y. Sun, L. Wang, X. Yu and K. Chen, *CrystEngComm*, 2012, **14**, 3199–3205.
- Z. Quanli, Y. Xiong and Y. Xie, *Inorg. Chem.*, 2003, **42**, 8105–8109.
- H. Zhang, D. Yang, Y. Ji, X. Ma, J. Xu and D. Que, *J. Phys. Chem. B*, 2004, **108**, 3955–3958.
- Z. Liu, H. Bai and D. D. Sun, *Int. J. Photoenergy*, 2012, **2012**, 1–11.
- Z. Guo, X. Chen, J. Li, J. H. Liu and X. J. Huang, *Langmuir*, 2011, **27**, 6193–6200.
- S.-J. Kim, C. W. Na, I.-S. Hwang and J.-H. Lee, *Sens. Actuators, B*, 2012, **168**, 83–89.
- A. Zainelabdin, G. Amin, S. Zaman, O. Nur, J. Lu, L. Hultman and M. Willander, *J. Mater. Chem.*, 2012, **22**, 11583–11591.
- E. G. Rochow, *J. Am. Chem. Soc.*, 1945, **67**, 963–965.
- D. Sun and B. E. Bent, *Catal. Lett.*, 1997, **46**, 127–132.
- J. Berzelius and F. A. Wöhler, *Organometallics*, 2001, **20**, 4978–4992.
- K. A. Magrini, J. L. Falconer and B. E. Koel, *J. Phys. Chem.*, 1989, **93**, 5563–5568.
- Z. Zhang, H. Che, Y. Wang, X. She, J. Sun, P. Gunawan, Z. Zhong and F. Su, *ACS Appl. Mater. Interfaces*, 2012, **4**, 1295–1302.
- L. N. Lewis, W. V. Ligon and J. C. Carnahan, *Silicon Chem.*, 2002, **1**, 23–33.
- Z. Zhang, H. Che, Y. Wang, J. Gao, X. She, J. Sun, Z. Zhong and F. Su, *RSC Adv.*, 2012, **2**, 2254–2259.
- R. Voorhoeve, B. Geertsem and J. C. Vlugter, *J. Catal.*, 1965, **4**, 43–47.
- M. K. Barr, T. M. Murphy and M. G. Williams, *USP-20050176981*, 2005.
- Z. Zhang, H. Che, J. Gao, Y. Wang, X. She, J. Sun, P. Gunawan, Z. Zhong and F. Su, *Catal. Sci. Technol.*, 2012, **2**, 1207–1212.
- A. D. Gordon, B. J. Hinch and D. R. Strongin, *Catal. Lett.*, 2009, **133**, 14–22.
- M. Chen, Y. Wang, L. Song, P. Gunawan, Z. Zhong, X. She and F. Su, *RSC Adv.*, 2012, **2**, 4164–4168.
- L. D. Gasper-Galvin, H. B. D. M. Sevenich, Fpiedrlch and D. G. Rethwlsch, *J. Catal.*, 1991, **128**, 468–478.
- B. Liu and H. C. Zeng, *J. Am. Chem. Soc.*, 2004, **126**, 8124–8125.
- L. N. Lewis and W. J. Ward, *Ind. Eng. Chem. Res.*, 2002, **41**, 397–402.
- Y. Liu, Y. Jiang, H. Yin, W. Chen, Y. Shen, Y. Feng, L. Shen, A. Wang, T. Jiang and Z. Wu, *Korean J. Chem. Eng.*, 2011, **28**, 2250–2254.
- L. N. Lewis, W. V. Ligon and J. C. Carnahan, *Silicon Chem.*, 2002, **1**, 23–33.
- Z. Liu, H. Bai, S. Xu and D. D. Sun, *Int. J. Hydrogen Energy*, 2011, **36**, 13473–13480.
- L. Wang, Y. Kang, Y. Wang, B. Zhu, S. Zhang, W. Huang and S. Wang, *Mater. Sci. Eng., C*, 2012, **32**, 2079–2085.
- Q. Simon, D. Barreca, A. Gasparotto, C. Maccato, T. Montini, V. Gombac, P. Fornasiero, O. I. Lebedev, S. Turner and G. Van Tendeloo, *J. Mater. Chem.*, 2012, **22**, 11739–11748.
- J. X. Wang, X. W. Sun, Y. Yang, K. K. Kyaw, X. Y. Huang, J. Z. Yin, J. Wei and H. V. Demir, *Nanotechnology*, 2011, **22**, 325704–325711.
- Y. Xu, D. Chen and X. Jiao, *J. Phys. Chem. B*, 2005, **109**, 13561–13566.
- L. Xu, S. Sithambaram, Y. Zhang, C. H. Chen, L. Jin, R. Joesten and S. L. Suib, *Chem. Mater.*, 2009, **21**, 1253–1259.
- P. W. Voorhees, *J. Stat. Phys.*, 1984, **38**, 231–252.
- J. Li and H. C. Zeng, *J. Am. Chem. Soc.*, 2007, **129**, 15839–15847.
- L. A. Gao and B. P. Ha, *J. Cryst. Growth*, 2007, **303**, 616–621.
- Q. Zhang, S.-J. Liu and S.-H. Yu, *J. Mater. Chem.*, 2009, **19**, 191–207.
- B. C. Lin, S. Y. Chen and P. Shen, *Nanoscale Res. Lett.*, 2012, **7**, 272–297.
- X. Jiang, G. Lu, R. Zhou, J. Mao, Y. Chen and X. Zheng, *Appl. Surf. Sci.*, 2001, **173**, 208–220.
- G. Fierro, M. L. Jacono, M. Inversi, p. Porta, F. Cioci and R. Lavecchia, *Appl. Catal., A*, 1996, **137**, 327–348.

- 51 Z. Zhang, L. M. Wong, H. G. Ong, X. J. Wang, J. L. Wang, S. J. Wang, H. Chen and T. Wu, *Nano Lett.*, 2008, **8**, 3205–3210.
- 52 T. J. Wessel and D. G. Rethwisch, *J. Catal.*, 1996, **161**, 861–866.
- 53 H. Ehrlich, D. Born, K. Richter, J. Richter-Mendau and H. Lieske, *Appl. Organomet. Chem.*, 1997, **11**, 237–247.
- 54 C. Xiao and F. Hagelberg, *THEOCHEM*, 2000, **529**, 241–257.
- 55 R. Larsson and B. Folkesson, *Acta Chem. Scand.*, 1996, **50**, 1060–1061.
- 56 M. K. Barr, C. NC, T. M. Murphy, A. NC, M. G. Willams and N. Raleigh, *USP-20050176981*, 2007.
- 57 J. M. Bablin, A. C. Crawford, D. C. DeMoulpied and L. N. Lewis, *Ind. Eng. Chem. Res.*, 2003, **42**, 3555–3565.
- 58 K. M. Lewis and J. S. Ritscher, *USP-7153991*, 2006.